Surface & Coatings Technology 203 (2009) 2793–2798

Contents lists available at ScienceDirect

Surface & Coatings Technology

journal homepage: www.elsevier.com/locate/surfcoat

Applications of plasma-based technology to microelectronics and biomedical engineering

Paul K. Chu *

Department of Physics and Materials Science, City University of Hong Kong, Tat Chee Avenue, Kowloon, Hong Kong, China

ARTICLE INFO

Available online 9 March 2009

Keywords:
Plasma immersion ion implantation and Deposition
Microelectronics
Silicon-on-insulator
Biomaterials
Titanium oxide

ABSTRACT

Plasma-based ion implantation and deposition techniques are widely used in many applications. In addition to the ability to modify the materials surface, novel structures can be fabricated. Another advantage is that the surface characteristics such as mechanical properties and biocompatibility can be selectively enhanced with the favorable bulk attributes of the materials unchanged. In this invited paper, our recent research activities on microelectronics and biomedical engineering are reviewed. Silicon-on-insulator (SOI) is expected to replace conventional bulk silicon substrates in many high speed, low power microelectronic devices because it possesses advantages such as reduction of parasitic capacitance, excellent sub-threshold slope, elimination of latch up, and resistance to radiation. However, wider applications of SOI in microelectronics are hampered by the self-heating effects caused by the poor thermal conductivity of the buried silicon dioxide layer. We have produced alternative buried insulators such as diamond-like carbon that possesses better thermal conductivity compared to conventional silicon dioxide using plasma immersion ion implantation and deposition (PIII&D) and successfully fabricated SOI structures with improved thermal stability. The use of low-energy plasma hydrogenation to substitute for the costly beam-line hydrogen ion implantation in the ion-cutting layer transfer technology is also discussed. In biomedical engineering, plasma spraying is a versatile technique to produce relatively thick ceramic coatings on orthopedic implant surfaces. We have discovered that plasma-sprayed nano-structured TiO_2 coatings favor the growth of apatite. The surface bioactivity is enhanced by hydrogen plasma implantation and the mechanism is discussed. The antibacterial properties of polymers can also be improved by implanting elements such as Ag and Cu and recent work in our laboratory is described.

©2009 Elsevier B.V. All rights reserved.

1. Introduction

Development of materials for deep-submicrometer microelectronic devices and novel biomaterials has benefited from plasma-based technologies. As device dimensions shrink, conventional bulk silicon wafers have deficiencies and thin silicon-on-insulator materials are especially suitable for microelectronic devices such as fully-depleted metal-oxide semiconductor field effect transistors (MOSFET) [1]. Recent results obtained in our laboratory pertaining to the production of novel silicon-on-insulator (SOI) materials to reduce the self-heating effects [2] are described. In the development of novel biomaterials, plasma-based nanotechnologies such as plasma immersion ion implantation offer the unique advantage that the surface properties and biocompatibility can be enhanced selectively while the favorable bulk characteristics of the materials remain unchanged [3,4]. For instance, mechanically sturdy materials with good wear and corrosion resistance can be modified to improve the surface bioactivity in biomedical applications. Existing materials can thus be used and needs for new classes of materials may be obviated thereby shortening the time to develop novel and better biomedical implants [5]. Recent works conducted in our laboratory pertaining to the improvement of surface bioactivity and antibacterial properties of biomaterials are reported.

2. Novel silicon-on-insulator (SOI) substrates for deep-submicrometer microelectronic devices

As the dimensions of metal oxide semiconductor field effect transistors (MOSFET) reach the nanometer regime, bulk silicon has some intrinsic deficiencies. Silicon-on-insulator (SOI) MOSFET is expected to replace conventional bulk silicon substrates in many microelectronic devices because it possesses many advantages such as reduction of parasitic capacitance, excellent sub-threshold slope, elimination of latch up, and resistance to radiation [6]. However, wider applications of SOI in ULSI are hampered by the self-heating effects caused by the poor thermal conductivity of the buried silicon dioxide layer [7]. We have recently explored alternative buried insulators with better thermal conductivity and successfully fabricated

* Tel.: +852 27887724; fax: +852 27889549 or +852 27887830.
E-mail address: paul.chu@cityu.edu.hk.

0257-8972/$ – see front matter ©2009 Elsevier B.V. All rights reserved.
doi:10.1016/j.surfcoat.2009.02.131

SOI structures using aluminum nitride or diamond-like carbon as the substitute for the buried silicon dioxide layer [8]. Fig. 1 shows the TEM micrograph of the SOD (silicon-on-diamond) structure fabricated in our laboratory showing successful formation of the SOD structure [9].

Fig. 2 shows the electrical breakdown fields of the SOD sample as a function of the annealing temperature. The breakdown field of the as-deposited diamond-like carbon (DLC) film is 4.2 MV/cm which compares reasonably well with previously reported results. When the samples are annealed in the furnace at temperatures under 900 °C, the breakdown fields do not change. When the annealing temperature reaches 900 °C, the breakdown field begins to decrease, but the changes are not obvious. However, when the temperature is increased to 1000 °C, the breakdown field diminishes significantly. It can be inferred that graphitization of our materials becomes significant at this temperature and our Raman results (not shown here) are consistent with the electrical measurements. The results (open circles in Fig. 2) indicate that after rapid thermal annealing (RTA) at 900 °C or 1000 °C, no appreciable graphitization can be detected from our electrical data. In accordance with our results, the DLC synthesized using the special PIII&D process can withstand furnace annealing and RTA up to 900 °C, and so the materials are compatible with thin film transistors (TFT) but not good enough for conventional CMOS processing.

High resistance against graphitization has been investigated and the presence of hydrogen in the DLC layer is observed to retard this deleterious process up to about 900 °C [10]. We compare the thermal

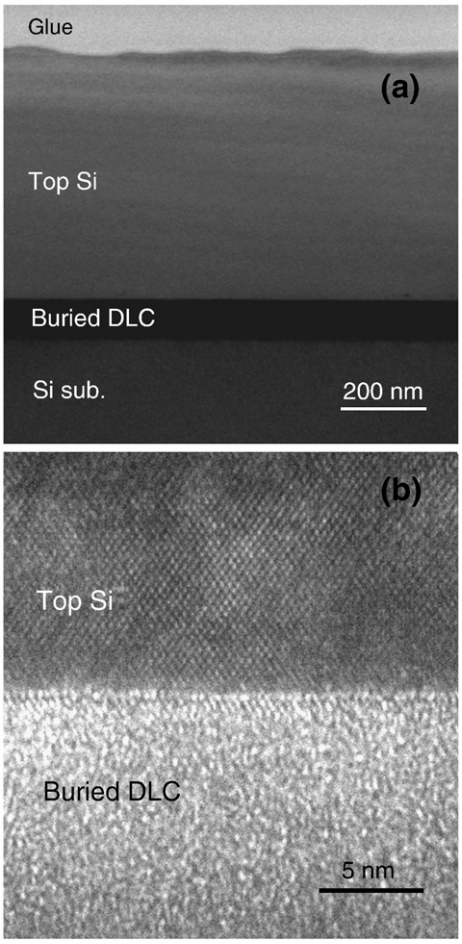

Fig. 1. (a) TEM micrograph of the SOD structure formed using direct wafer bonding and hydrogen-induced layer transfer. (b) HRTEM micrograph of the interfacial region between the top Si layer and buried DLC layer, indicating a defect-free and single crystal Si layer as well as an abrupt bonded interface.

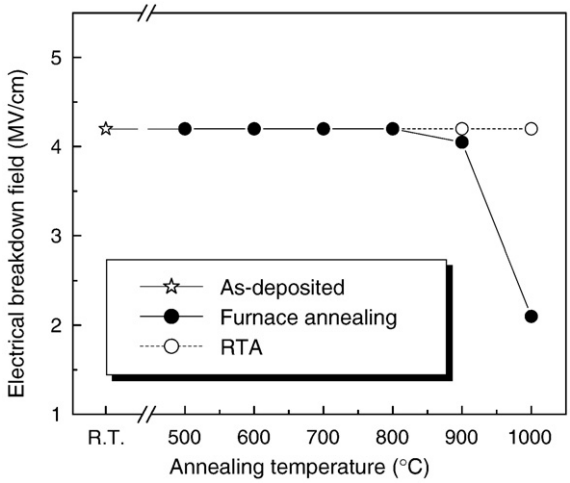

Fig. 2. Influence of the annealing temperature on the electrical breakdown fields for the DLC films. Filled and open circles represent results from furnace annealing and RTA in nitrogen ambient. The star is for the as-deposited sample.

stability of exposed and buried DLC films using Raman spectroscopy and X-ray photoelectron spectroscopy (XPS). Our Raman analysis indicates that the obvious separation of the D and G peaks indicative of nano-crystalline graphite emerges at 500 °C in the exposed DLC film. In contrast, the separation appears in the buried DLC film only at annealing temperatures above 800 °C. Analysis of the XPS C_{1s} core level spectra shows that the (sp^3 + C–H) carbon content of the unprotected DLC film decreases rapidly between 300 and 700 °C indicating the rapid transformation of sp^3-bonded carbon to sp^2-bonded carbon combined with hydrogen evolution. In comparison, the decrease in the (sp^3 + C–H) carbon content in the buried DLC film is slower below 800 °C. Elastic recoil detection (ERD) results show that this superior thermal stability is due to the slower hydrogen outdiffusion from the buried DLC film thereby impeding the graphitization process. Our results thus show that the SiO_2 overlayer retards

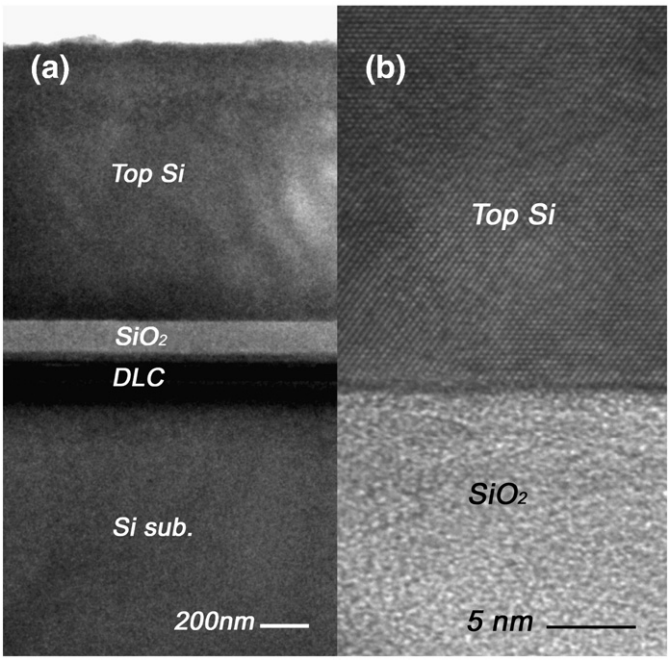

Fig. 3. (a) TEM micrograph of the SiO_2/DLC SODI structure. (b) HRTEM micrograph of the interfacial region between the top Si layer and buried insulator structure showing a sharp Si/SiO_2 interface and defect-free crystalline Si layer.

the graphitization process during annealing by shifting the chemical equilibrium.

Hence, in order to produce SOI materials with both good thermal conductance and thermal stability, our proposed solution is to introduce a thin silicon dioxide barrier layer between the Si film and DLC buried layer to form a silicon-on-SiO_2/DLC dual-insulator (SODI) structure [11]. The cross-section of such a structure is displayed in Fig. 3. A resistive buried layer is imperative to the optimal operation of SOI devices and so we also measure the breakdown electric fields of our SODI sample at various temperatures to determine the thermal stability. As shown in Fig. 4, even at an annealing temperature as high as 1000 °C, the breakdown field of 4.6 ± 0.1 MV/cm remains unchanged thereby showing improvement over the SOD structure described previously. The enhanced property is believed to be due to two reasons. Firstly, the SiO_2 layer has high thermal stability and secondly, the SiO_2 layer blocks hydrogen out-diffusion from the DLC layer.

In the conventional ion-cutting technology, hydrogen is implanted into the donor silicon wafer either by the beam-line or plasma immersion technique. In spite of the small mass of hydrogen ions, implantation inevitability causes substrate damage which can adversely impact device yields and high-dose hydrogen implantation also tends to be costly. We have thus explored the possibility of using low-energy hydrogen plasma hydrogenation instead of hydrogen ion implantation to perform ion-cutting and layer transfer to produce SOI [12,13]. Boron ion implantation is used to introduce H-trapping centers into Si wafers to illustrate the idea. Instead of the widely recognized interactions between boron and hydrogen atoms, our results impart that lattice damage, i.e., dangling bonds, traps H atoms and can lead to surface blistering during hydrogenation or upon post-annealing at higher temperatures. Boron ion implantation and subsequent processes control the uniformity of H-trapping and the trapping depths. While the trapping centers are introduced by B ion implantation in this study, there are many other means to do the same without implantation. Using this technology, we have successfully fabricated SOI structure using this novel technology, as shown in Fig. 5 [14]. Our process starts with p-type 1–35 Ω cm <111> Si wafers. A dose of 5×10^{15} cm^{-2} B^+ is implanted into the Si substrates at 170 kV, followed by boron activation at 900 °C in N_2 for 20 min. Plasma hydrogenation is conducted at 280 °C in a plasma immersion ion implanter (PIII) with a radio frequency (RF) plasma source for 10 min [15]. These conditions are selected to introduce sufficient hydrogen atoms into the substrates but without causing surface blistering to arise directly after plasma hydrogenation. After Ar plasma activation of the sample surface, the hydrogenated sample is bonded to a Si handle wafer with an oxide top layer. Finally, the bonded structure is thermally annealed at 400 °C to induce Si layer splitting and transfer, yielding the SOI structure exhibited in Fig. 5.

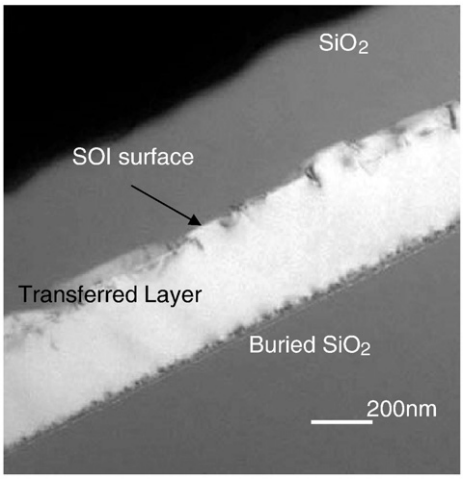

Fig. 5. Cross-section transmission electron micrographs obtained from the final SOI sample fabricated by plasma hydrogenation combined with wafer bonding.

3. Nano-structured biomaterials

Surfaces play an important role in the response of the biological environment to artificial medical devices such as implants [16–18]. The physical, chemical, and biochemical properties of the implant surface control performance-relevant processes such as protein adsorption, cell–surface interaction, and cell/tissue development at the interface between the body and the biomaterials. Nano-sized surface topography may render biomedical implants with special and favorable properties in a biological environment. For instance, it has been shown that nanophase ceramics can promote osseointegration that is critical to the clinical success of orthopedic/dental implants [19]. Osteoblast proliferation is observed to be significantly higher on nanophase alumina, titania, and hydroxyapatite (HA) in comparison to their conventional counterparts.

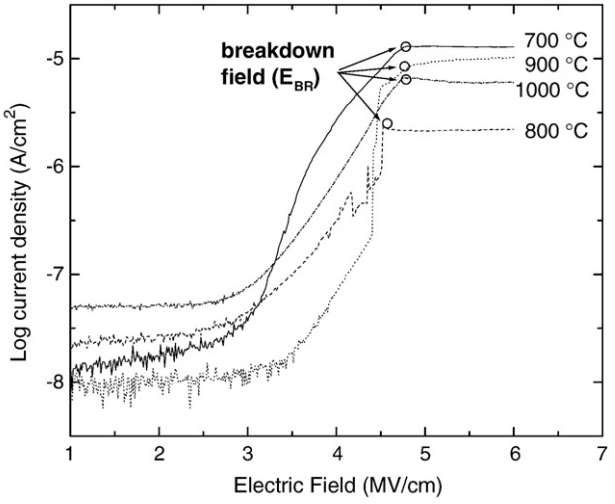

Fig. 4. Influence of the annealing temperature on the breakdown electric fields of the SODI structure.

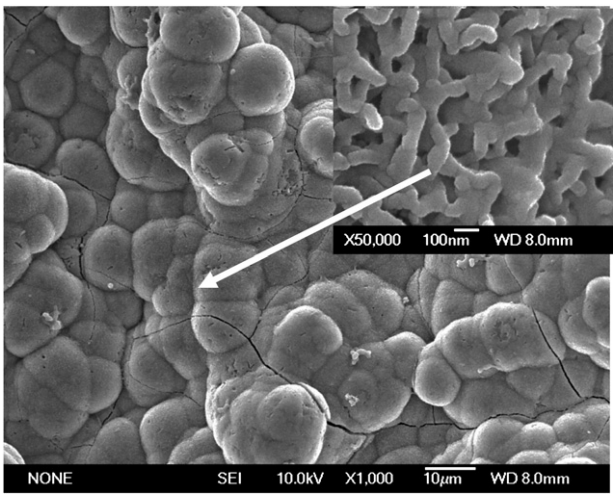

Fig. 6. Surface SEM views of the hydrogen-PIII nano-TiO_2 coating after soaking in SBF for two weeks (upper right corner shows the low-magnification image).

In biomedical applications, although some types of TiO_2 powders and gel-derived films can exhibit bioactivity, plasma-sprayed TiO_2 coatings [20,21] are always bioinert, thereby hampering wider applications in bone implants. Recently, we have successfully produced a bioactive nano-structured TiO_2 surface with grain size smaller than 50 nm using nano-particle plasma spraying followed by hydrogen plasma immersion ion implantation (PIII) [22]. After immersion in simulated body fluids (SBF) for two weeks, the surface of the hydrogen-PIII nano-TiO_2 coating is completely covered by a newly-formed layer, as shown in the surface micrographs depicted in Fig. 6. At a higher magnification, the newly-formed layer exhibits a subtle net-like structure consisting of nano-sized rods. The cross-sections of the hydrogen-PIII nano-TiO_2 coating immersed in SBF for two and four weeks reveal that the newly-formed layer is Ca and P rich with a thickness of about 5 μm after two weeks and about 25 μm after four weeks, as shown in Figs. 7 and 8. The XRD and FTIR results (not shown here) indicate that the new layer formed on the hydrogen-PIII nano-TiO_2 coating consists of carbonate-containing hydroxyapatite. In contrast, in our control experiments involving the as-sprayed nano-TiO_2 and micro-TiO_2 coatings as well as the hydrogen-PIII micro-TiO_2 coating and hydrogen-PIII polished nano-TiO_2 coating in which the nano-structured surface is removed, no new precipitates can be detected after the samples are soaked in SBF for two weeks, as shown in Fig. 9.

Our results show that the hydrogen-PIII nano-TiO_2 coating can induce bone-like apatite formation on its surface after immersion in simulated body fluids. On the other hand, apatite cannot form on either the as-sprayed TiO_2 surfaces (both <50 nm grain size and >50 nm grain size) or hydrogen-implanted TiO_2 with grain sizes larger than 50 nm. Therefore, both a hydrogenated surface that leads to negatively-charged functional groups on the surface and small grain size (<50 nm) that enhances surface adsorption are critical to the growth of apatite. Introduction of surface bioactivity to plasma-sprayed TiO_2 coatings which are generally recognized to have excellent biocompatibility and corrosion resistance as well as high bonding strength to titanium alloys makes them superior to many current biomedical coatings.

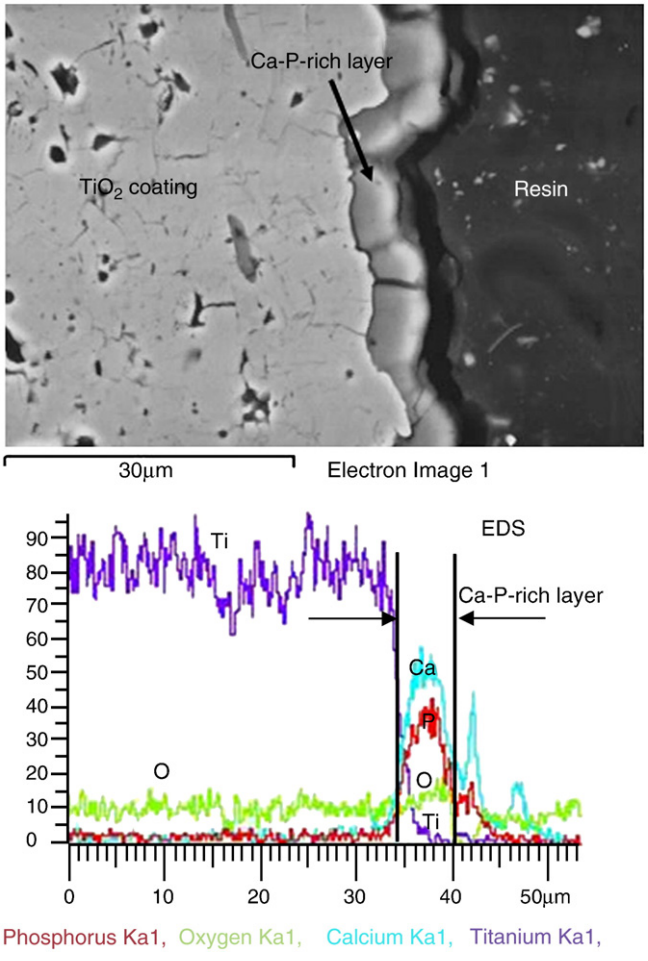

Fig. 7. Cross-sectional SEM views and EDS analysis of the hydrogen-PIII nano-TiO_2 coating after soaking in SBF for two weeks.

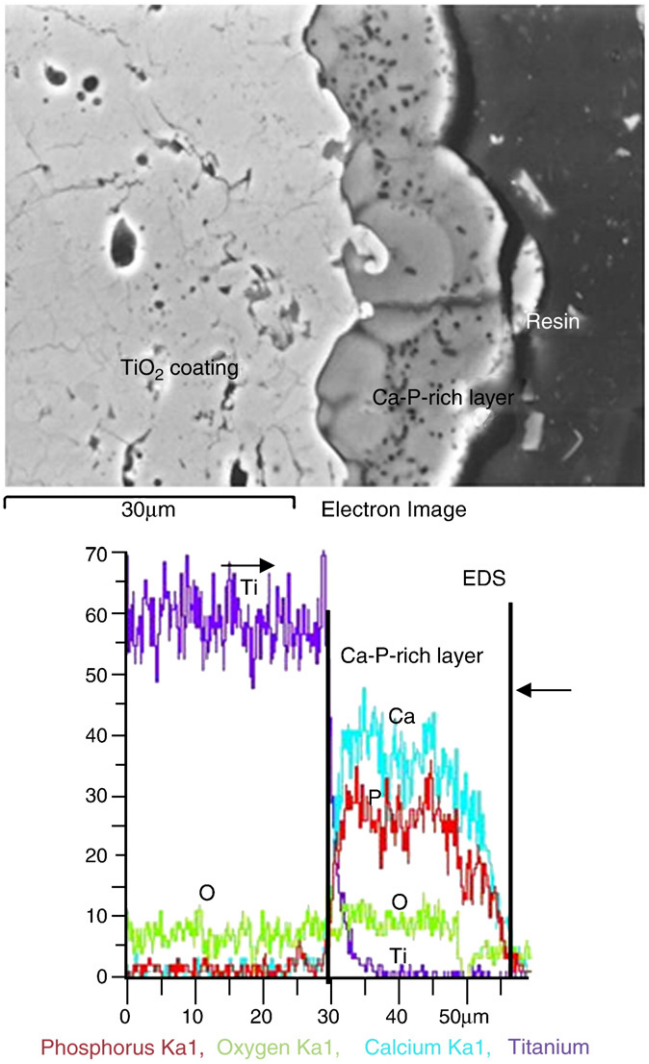

Fig. 8. Cross-sectional SEM views and EDS analysis of the hydrogen-PIII nano-TiO_2 coating after soaking in SBF for four weeks.

The surface of the TiO_2 coating produced from the nano-particles is composed of particles less than 50 nm in size, whereas the surface of the TiO_2 coating produced from the submicrometer-particles consists of particles larger than 50 nm. X-ray diffraction reveals that both coatings have primarily the rutile structure with a small amount of anatase and TiO_{2-x} suboxide (most of them is Ti_3O_5). However, the phase compositions of their outermost layer are mostly anatase. After hydrogen PIII, the nano-TiO_2 coating exhibits excellent bioactivity. The hydrogen-PIII nano-TiO_2 coating can induce carbonate-containing hydroxyapatite formation on its surface in simulated body fluids, but carbonate-containing hydroxyapatite cannot form on either the as-sprayed TiO_2 surfaces (both <50 nm grain size and >50 nm grain size) or hydrogen-implanted TiO_2 with grain sizes larger than 50 nm.

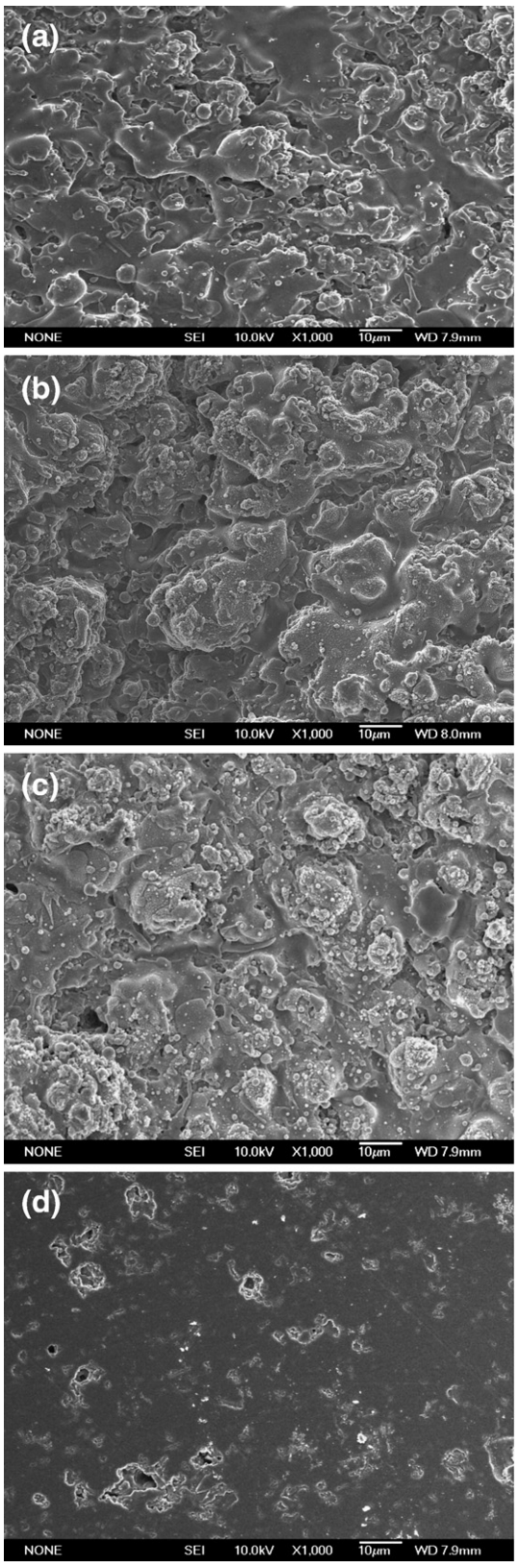

Fig. 9. SEM plan-views of various TiO_2 coatings soaked in SBF for two weeks: (a) as-sprayed nano-TiO_2 coating, (b) as-sprayed micro-TiO_2 coating, (c) hydrogen-PIII micro-TiO_2 coating and (d) hydrogen-PIII polished nano-TiO_2 coating (the nano-structured surface is removed).

There is strong evidence that the bioactivity of the plasma-sprayed TiO_2 coating depends on a nano-structured surface composed of enough small particles in addition to hydrogen incorporation which yields the favorable surface functional groups for carbonate-containing hydroxyapatite formation.

4. Antibacterial properties of plasma-implanted polymers

Polymers are common medical materials because of their superior properties such as easy processing, ductility, impact load damping, and excellent bio-comparability [23–25]. However, infection of medical polymers by microbes is one of the major clinical complications causing a high rate of mortality [26,27]. The two conventional methods to enhance the surface anti-infection properties of medical polymers are deposition of an antibacterial coating and/or introduction of an antibacterial reagent into the polymer matrix [28–30]. However, these techniques suffer drawbacks such as temporary and unstable antibacterial effects as well as fast consumption of the antibacterial reagents. One way to overcome these obstacles is to introduce an organic or inorganic antibacterial reagent such as Cu into the subsurface region by plasma immersion ion implantation [31–34].

Here, we describe our recent work on Cu PIII to improve the antibacterial properties of medical polyethylene (PE). Copper is an excellent antimicrobial agent but since it does not bond with the PE matrix, leaching of implanted Cu can be quite fast thereby reducing the long term antibacterial effects. Our recent experiments reveal that gaseous ion co-implantation in concert with Cu PIII can regulate the copper release rate from the substrates and enhance the long term effects [35,36]. In particular, nitrogen co-PIII produces the best results. Fig. 10 shows that a relatively large amount of Cu leaches into the SBF from all four plasma treated samples (sample 1 — control, sample 2 — Cu/NH_3 PIII, sample 3 — Cu/O_2 PIII, and sample 4 — Cu/N_2 PIII) after the first 2 days, primarily arising from the surface Cu and the Cu release rate diminishes afterwards. Compared to the Cu PIII PE sample (sample 1), the O_2 and N_2 plasma co-implanted samples (samples 3 and 4) show reduced Cu leaching rates. Our results indicate that both N_2 and O_2 PIII can regulate Cu out-diffusion and give rise to steadier release rates.

The appearance of the peak at 1598.5 cm^{-1} in the Raman spectra of samples 2 and 3 (not shown here) suggests dehydrogenation and conversion of sp^3 into sp^2 C along the polyethylene chain. However, this peak is not detected from sample 4, implying less dehydrogenation and formation of CC and C≡N bonds. The CC and C≡N bonds are more polar and believed to hold onto Cu atoms more effectively.

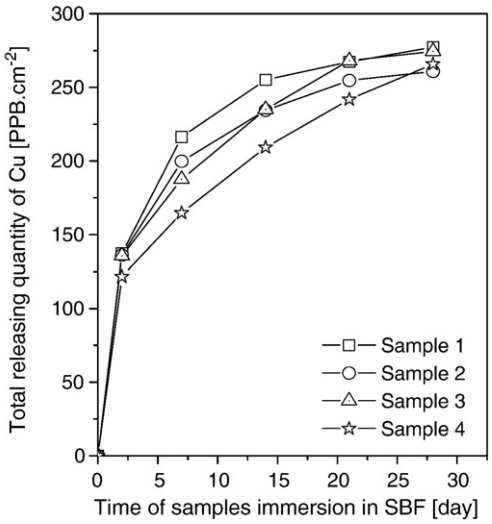

Fig. 10. Cumulative amounts of Cu released into the SBF from four plasma-implanted samples after immersion times of 2, 7, 14, 21, and 28 days (sample 1 — control, sample 2 — Cu/NH_3 PIII, sample 3 — Cu/O_2 PIII, and sample 4 — Cu/N_2 PIII). The SBF was replenished after each sampling.

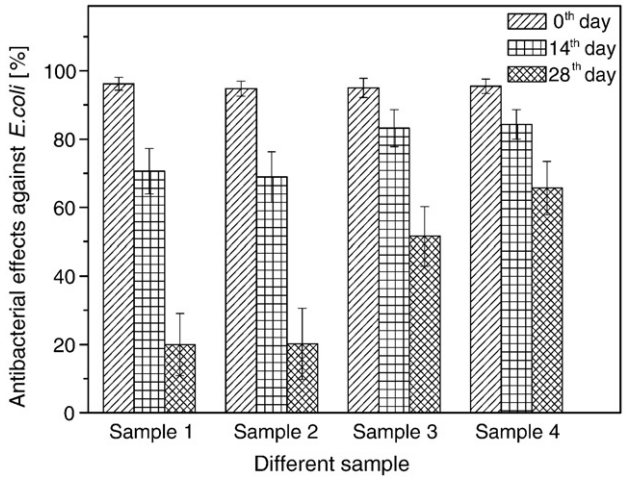

Fig. 11. Antibacterial effectiveness against *E. coli* after immersion times of 0, 14, and 28 days (sample 1 — control, sample 2 — Cu/NH_3 PIII, sample 3 — Cu/O_2 PIII, and sample 4 — Cu/N_2 PIII).

Consequently, a smaller release rate of Cu is observed during the first two days of immersion, and the release rate is steadier subsequently. Although both the NH_3 and N_2 plasmas introduce N into the PE samples, the effects are different. It may be because –C–NH_3 and –CNH groups are formed in the substrate due to scission of NH_3 according to the following possible reaction:

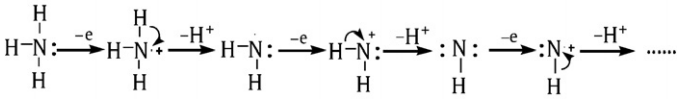

The C–NH_3 groups have saturated bonds and are ineffective in detaining Cu and are believed to be the reason why the Cu diffusion rate in sample 2 is higher than those in samples 3 and 4 in the beginning. It is believed that the altered chemistry plays a crucial role in the Cu diffusion mechanism.

E. coli is employed to assess the antimicrobial properties of the plasma-implanted samples for various immersion times of 0, 14, and 28 days. As shown in Fig. 11, all four samples exhibit excellent antibacterial effects (>95%) against *E. coli* with a cell concentration of 10^6 CFU/ml initially (day 0). Cu PIII can thus provide immediate antimicrobial effects and the antibacterial effectiveness of all the samples diminishes with immersion times. Samples 3 and 4 show better antibacterial performance compared to samples 1 and 2, and the data agree with the Cu release trend illustrated in Fig. 10.

5. Conclusion

Plasma-based technologies such as plasma immersion ion implantation and deposition are gaining acceptance by the microelectronics and biomedical industry. In this paper, recent works on the production of novel silicon-on-insulator structures such as silicon-on-diamond (SOD) and silicon-on-dual-insulator (SODI) that are not as vulnerable to self-heating effects as conventional silicon dioxide-based SOI structures and the use of plasma hydrogenation to effect layer transfer are described. The use of nano-particle plasma spraying in conjunction with hydrogen plasma immersion ion implantation produces bioactive TiO_2 coatings which bode well for tissue integration in orthopedic applications. Last and the least, PIII can introduce an inorganic antimicrobial agent such as Cu into an organic matrix such as polyethylene to produce reliable antibacterial effects which can be improved by co-implantation of a gas element such as nitrogen.

Acknowledgement

The work was financially supported by Hong Kong Research Grants Council (RGC) Competitive Earmarked Research Grant (CERG) No. CityU 112306.

References

[1] B.G. Streetman, S. Banerjee, Solid State Electronic Devices, 5th EditionPrentice Hall, New Jersey, 2000.
[2] W. Redman-Whire, M.S.L. Lee, B.M. Tenbroek, M.J. Uren, R.J.T. Bunyan, Electron. Lett. 29 (1993) 1180.
[3] A. Anders (Ed.), Handbook of Plasma Immersion Ion Implantation and Deposition, Wiley, New York, 2000.
[4] P.K. Chu, J.Y. Chen, L.P. Wang, N. Huang, Mater. Sci. Eng., R Rep. 36 (2002) 143.
[5] P.K. Chu, Surf. Coat. Technol. 201 (2007) 5601.
[6] J.P. Colinge, Silicon-on-Insulator Technology: Materials to VLSI, Kluwer, Boston, 1991.
[7] P.K. Chu, IEEE Circuits and Systems Magazine, 2005, pp. 16–27, Fourth Quarter.
[8] M. Zhu, P. Chen, R.K.Y. Fu, Z.H. An, C.L. Lin, P.K. Chu, IEEE Trans. Electron Devices 51 (2004) 901.
[9] M. Zhu, P.K. Chu, X. Shi, M. Wong, W.L. Liu, C.L. Lin, Appl. Phys. Lett. 85 (2004) 2532.
[10] Z.F. Di, A.P. Huang, R.K.Y. Fu, P.K. Chu, L. Shao, T. Höchbauer, M. Nastasi, M. Zhang, W.L. Liu, Q.W. Shen, S.H. Luo, Z.T. Song, C.L. Lin, J. Appl. Phys. 98 (2005) 053502.
[11] Z.F. Di, P.K. Chu, M. Zhu, R.K.Y. Fu, S.H. Luo, L. Shao, M. Nastasi, P. Chen, T.L. Alford, J.W. Mayer, M. Zhang, W.L. Liu, Z.T. Song, C.L. Lin, Appl. Phys. Lett. 88 (2006) 142108.
[12] P. Chen, P.K. Chu, T. Höchbauer, J.-K. Lee, M. Nastasi, D. Buca, S. Mantl, R. Loo, M. Caymax, T. Alford, J.W. Mayer, N.D. Theodore, M. Cai, B. Schmidt, S.S. Lau, Appl. Phys. Lett. 86 (2005) 031904.
[13] L. Shao, Y. Lin, J.K. Lee, Q.X. Jia, Y.Q. Wang, M. Nastasi, P.E. Thompson, N.D. Theodore, P.K. Chu, T.L. Alford, J.W. Mayer, P. Chen, S.S. Lau, Appl. Phys. Lett. 87 (2005) 091902.
[14] P. Chen, S.S. Lau, P.K. Chu, K. Henttinen, T. Suni, I. Suni, N.D. Theodore, T. Alford, J.W. Mayer, L. Shao, M. Nastasi, Appl. Phys. Lett. 87 (2005) 111910.
[15] P.K. Chu, S. Qin, C. Chan, N.W. Cheung, L.A. Larson, Mater. Sci. Eng., R Rep. 17 (1996) 207.
[16] H.M. Kim, F. Miyaji, T. Kokubo, S. Nishiguchi, T. Nakamura, J. Biomed. Mater. Res. 45 (1999) 100.
[17] N. Moritz, M. Jokinen, T. Peltola, S. Areva, A. Yli-Urpo, J. Biomed. Mater. Res. 65A (2003) 9.
[18] X. Liu, R.K.Y. Fu, R.W.Y. Poon, P. Chen, P.K. Chu, C. Ding, Biomaterials 25 (2004) 5575.
[19] T.J. Webster, C. Ergun, R.H. Doremus, R.W. Siegel, R. Bizios, Biomaterials 22 (2001) 1327.
[20] M. Keshmiri, T. Troczynski, J. Non-cryst. Solids 324 (2003) 289.
[21] T. Peltola, M. Jokinen, H. Rahiala, M. Ptsi, J. Heikkilä, I. Kangasniemi, A. Yli-Urpo, J. Biomed. Mater. Res. 51 (2000) 200.
[22] X.Y. Liu, X.B. Zhao, R.K.Y. Fu, J.P.Y. Ho, C.X. Ding, P.K. Chu, Biomaterials 26 (2005) 6143.
[23] A.S. Luyt, J.A. Molefi, H. Krump, Polym. Degrad. Stab. 91 (2006) 1629.
[24] J.C. Middleton, A.J. Tipton, Biomaterials 21 (2000) 2335.
[25] N.M.K. Lamba, J.M. Courtney, J.D.S. Gaylor, G.D.O. Lowe, Biomaterials 21 (2000) 89.
[26] Y.H. An, R.J. Friedman, J. Biomed. Mater. Res. 43 (1998) 338.
[27] I.B. Beech, J.R. Smith, A.A. Steele, Colloids Surf., B Biointerfaces 23 (2002) 231.
[28] J. Thome, A. Holländer, W. Jaeger, I. Trick, C. Oehr, Surf. Coat. Technol. 174–175 (2003) 584.
[29] D.P. Dowling, A.J. Betts, C. Pope, M.L. McConnell, R. Eloy, M.N. Arnaud, Surf. Coat. Technol. 163–164 (2003) 637.
[30] B.D. Kalyon, U. Olgun, Am. J. Infect. Control 29 (2001) 124.
[31] R.K.Y. Fu, I.T.L. Cheung, Y.F. Mei, C.H. Shek, G.G. Siu, P.K. Chu, W.M. Yang, Y.X. Leng, Y.X. Huang, X.B. Tian, S.Q. Yang, Nucl. Instrum. Methods Phys. Res., B Beam Interact. Mater. Atoms 237 (2005) 417.
[32] W. Zhang, P.K. Chu, J.H. Ji, Y.H. Zhang, Appl. Surf. Sci. 252 (2006) 7884.
[33] W. Zhang, Y.H. Zhang, J.H. Ji, J. Zhao, P.K. Chu, Q. Yan, Polymer 47 (2006) 7441.
[34] W. Zhang, P.K. Chu, J.H. Ji, Y.H. Zhang, Q. Yan, Biomaterials 27 (2006) 44.
[35] W. Zhang, J.H. Ji, Y.H. Zhang, Q. Yan, E.Z. Kurmaev, A. Moewes, J. Zhao, P.K. Chu, Appl. Surf. Sci. 253 (2007) 8981.
[36] W. Zhang, J.H. Ji, Y.H. Zhang, Q. Yan, P.K. Chu, Plasma Processes Polym. 4 (2007) 158.